Journal of Sensor Science and Technology
Vol. 33, No. 2 (2024) pp. 63-69
http://dx.doi.org/10.46670/JSST.2024.33.2.63
pISSN 1225-5475/eISSN 2093-7563

Solid Electrochemical Method of Measuring Hydrogen Concentration with O2-/H+ Hetero-Ionic Junction

Chongook Park[1,+]

Abstract

A novel method for measuring hydrogen concentration is introduced, along with its working principle and a novel detection algorithm. This configuration requires no additional reference compartment for potentiometric electrochemical measurements; therefore, it is the most suitable for measuring dissolved hydrogen in the liquid phase. The sensor's electromotive force saturates at a certain point, depending on the hydrogen concentration during the heating process of the sensor operation. This dynamic temperature scanning method provides higher sensitivity than the constant temperature measurement method.

Keywords: Solid electrolyte, Hydrogen, Sensor, Proton conductor, Oxygen ion conductor

1. INTRODUCTION

The dominant energy source changes from carbon to hydrogen someday [1]. Hydrogen detection and concentration measurement are necessary during production, storage, and transportation in this emerging hydrogen economy. Therefore, there is an ongoing need for faster, more durable, more accurate, and more selective hydrogen gas detection in various industrial areas to monitor and control hydrogen concentration. For example, monitoring the hydrogen gas concentration is important in the synthesis of chemicals such as ammonia, methanol, and rocket fuels in the Al foundry, in the welding and galvanic plating processes to avoid hydrogen embrittlement, in the detection of impending electric transformer failure, in the lighting industry to check the hydrogen impurities in krypton, xenon, and neon, and in nuclear power plants to prevent hydrogen explosions.

Many commercially available sensors have been reported for hydrogen detection. According to their operating principles, these can be classified as chemoresistive sensors [2-4], fuel cell sensors [5,6], FET sensors [7], Pd resistor sensors [8], and mixed potential sensors [9]. Each type has advantages and disadvantages and serves well in its applications. However, it may be difficult to find an appropriate hydrogen sensor in harsh environments, such as high temperatures or polluted sites. The measurement of dissolved hydrogen in hot melts or volatile industrial oils may be such a case.

Iwahara [10] first adopted a proton-conducting solid electrolyte, $CaZr_{0.9}In_{0.1}O_{3-x}$ (CZI), to build a hydrogen sensor for an Al melt. In this potentiometric configuration, hydrogen gas with a known concentration must flow into the reference compartment to detect the dissolved hydrogen in the Al melt. Later, Schwandt [11] introduced a solid-state hydrogen sensor with a solid reference to a Ti and TiHx mixture in an Al melt. This study introduced a novel solid electrochemical hydrogen sensor that operates without a flowing reference gas. To operate this sensor, a novel sensing method is devised whereby a momentary electromotive force (EMF) is detected along with its temperature while the sensor is being heated for a given hydrogen concentration, which is called the dynamic temperature scanning method (DTSM) here.

1.1 Operating Principle

The newly developed structure of the hydrogen measuring cell can be written as

$$(-)\ H_2,\ Pt\ |CaZr_{0.9}In_{0.1}O_{3-x}H_y\ ||YSZ\ |Pt,\ Air\ (O_2)\ (+) \qquad (1)$$

The oxygen ions are in equilibrium with the oxygen at the Pt/YSZ electrode via Eq. 2 and combine with protons in the proton conductor to form a so-called water potential at the YSZ (yttria-stabilized zirconia)/CZI ($CaZr_{0.9}In_{0.1}O_{3-\delta}$) interface as in Eq. 3. At the working electrode, hydrogen in the gas phase and protons on the CZI surface maintained equilibrium with the electrons in Pt, as

[1]PSS Inc.
Unit 206, Building B, Techno 4-ro, Yuseong-gu, Daejeon, Republic of Korea
[+]Corresponding author: copark@kaist.ac.kr
(Received: Oct. 30, 2023, Accepted: Nov. 7, 2023)

expressed in Eq. 4.

$$\frac{1}{2}O_2 + 2e^- (Pt) = O^{2-} (YSZ) \quad (2)$$

$$2H^+(CZI) + O^{2-}(YSZ) = H_2O \quad (3)$$

$$H_2 = 2H^+(CaZr_{0.9}In_{0.1}O_{3-\delta}) + 2e^-(Pt) \quad (4)$$

Thus, the overall reaction of the cell can be described with Eq. 5.

$$H_2 + \frac{1}{2}O_2 = H_2O \quad (5)$$

According to the Nernst relation, $E = -\Delta G/2F$ the EMF of electrochemical Cell 1 can be represented as:

$$E = -\frac{\Delta G^o_{H_2O}}{2F} - \frac{RT}{2F}\ln\frac{a_{H_2O}}{P_{H_2}P_{O_2}^{1/2}} \quad (6)$$

where $\Delta G^o_{H_2O} = -247500 + 55.85T$ J/mol [20], F, a_{H_2O}, P_{H_2}, and $P_{O_2}^{1/2}$ are the standard Gibbs free energy of water formation, Faraday constant, activity of water at the YSZ/CZI interface, hydrogen partial pressure at the measuring electrode, and oxygen partial pressure at the reference electrode, respectively.

The reference electrode can be either a Pt/YSZ electrode simply exposed to open air or contained in a closed chamber that is hermetically sealed and filled with a metal and metal oxide mixture, such as CuO/Cu_2O and Ni/NiO, to maintain a constant oxygen pressure.

The water activity at the CZI/YSZ interface was experimentally measured by changing both temperature and hydrogen environment with the known value of $\Delta G^o_{H_2O}$ [12]. They demonstrated almost constant values within the tested ranges of temperature and hydrogen concentration, as illustrated in Fig. 1. However, the thermodynamic activity of water in the proton conductor could not be fixed [13]. Water is believed to be formed at the YSZ/CZI interface, which is determined by the oxygen ions in the YSZ and protons in the CZI. They are tightly bonded and resistant to small perturbations. Further studies on this interface are required. Therefore, for constant a_{H_2O} and p_{O_2}=0.21, Eq. 6 can be simplified as

$$E = E_0' + \frac{RT}{2F}\ln P_{H_2} \quad (7)$$

where E_0' corresponds to $(-\Delta G^o_{H_2O}/2F - RT/2F \ln a_{H_2O} + RT/4F \ln P_{O_2})$. Because $\Delta G^o = \Delta H^o - T\Delta S^o$, E_0' would be a function of temperature. It experimentally demonstrates a small dependence on temperature with a slope of -2.46 × 10^{-4}, as illustrated in Fig. 2 [14], which is close to the thermodynamically

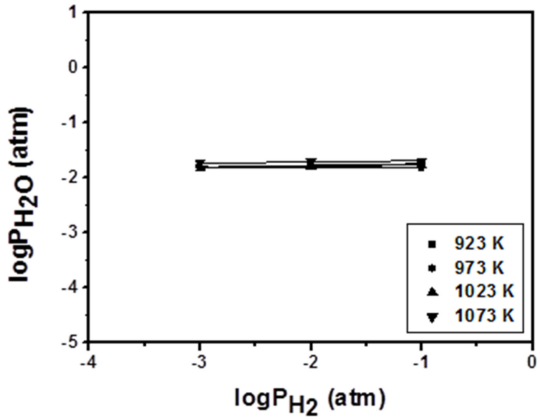

Fig. 1. Change of water potential at interface with hydrogen pressure at different temperatures

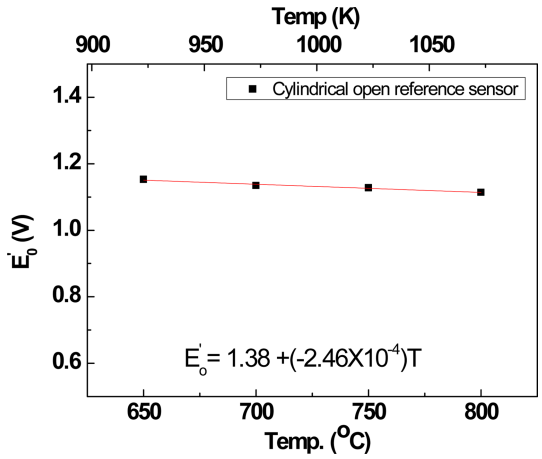

Fig. 2. E_0' as function of temperature.

calculated value (=$\Delta S^o_{H_2O}/2F$) of -2.89 × 10^{-4}. Consequently, the cell EMF can be expressed by Eq. 8.

$$E = A + BT + CT\log p_{H_2} \quad (8)$$

where A, B, and C are sensor constants. According to Eq. 8, the EMF is a function of the temperature and hydrogen pressure. Thus, hydrogen concentration can be calculated by substituting the measured temperature and EMF into Eq. 8 with known sensor constants A, B, and C.

1.2. General Gas Response of Sensor

The sensor responds quite well to changes in hydrogen gas concentration from 0.1% to 10% H_2 in nitrogen for a wide temperature ranging from 650 to 800 °C in the laboratory test as illustrated in Fig. 3(a). Plotting the EMF vs $\log p_{H_2}$ according to Eq. 8 for a given temperature exhibited good Nernstian behavior with an almost theoretical slope, as illustrated in Fig. 3(b).

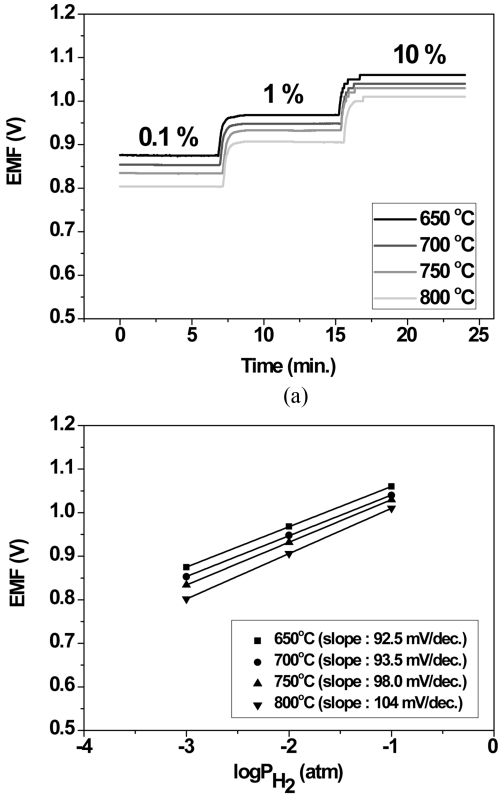

Fig. 3. EMF response of Cell 1 at temperature ranging from 650 to 800 °]C: (a) transient behavior and (b) EMF vs logarithm of hydrogen partial pressure.

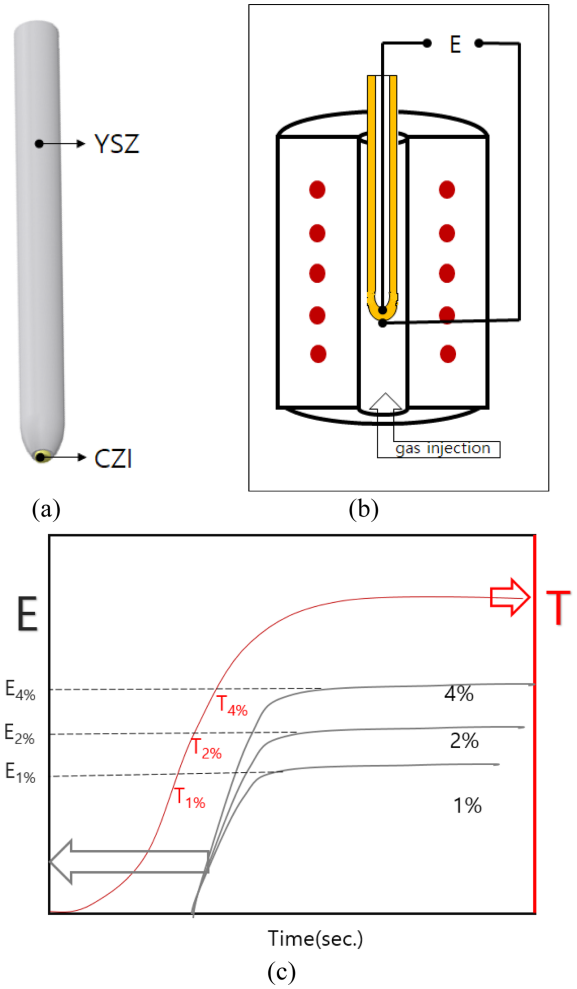

Fig. 4. (a) hetero ionic junction Sensor, (b) sensor testing set-up and (c) data acquisition

2. EXPERIMENTAL

A heterojunction sensor was fabricated by attaching a CZI pellet to the tip of a YSZ tube, as illustrated in Fig. 4(a). The vertical furnace was maintained at the desired temperature and a known concentration of hydrogen gas was introduced from the bottom, as illustrated in Fig. 4(b). As soon as the gas environment stabilized in a quartz tube placed inside the furnace, the sensor was immersed in a quartz tube to measure the EMF and temperature of the sensor with a data logger (Agilent 34970A). The typical behavior of the EMF and temperature of the sensor is illustrated in Fig. 4(c), where the temperature is on the right side and the EMF is on the left side. From a series of measurements, we obtained data for the corresponding hydrogen concentration, for example, Ei, Ti, and %H_2.

2.1 Mathematical Understanding of Response

As indicated in Eq. 8, the output from Sensor E is a function of T and log[H_2] with three constants: A, B, and C. Assuming a known hydrogen concentration, Eq. 8 becomes a function of T and is expressed as

$$E=A+C\{\log[H2]+B/C\}T=A+B'T \quad (9)$$

where log[H_2] is no longer a variable but a constant. Thus, depending on the hydrogen concentration, the EMF followed a different dotted line in the E vs. T plot, as illustrated in Fig. 7(a). The isohydrogen concentration line (dotted line) increased with the hydrogen concentration. Similarly, for Constant T, Eq. 8 can be rearranged as a function of log[H_2] as follows.

$$E=A+CT\{\log[H_2]+B/C\} \quad (10)$$

For simplicity, if log[H_2]+B/C is set to x, Eq. 10 becomes a first-order linear equation of E=A+C′x where C′= C{log[H_2]+B/C}. Accordingly, it gives isothermal lines (dotted) on which the EMF varies with hydrogen concentration at a given temperature, as illustrated in Fig. 7(b). As the temperature increases, the

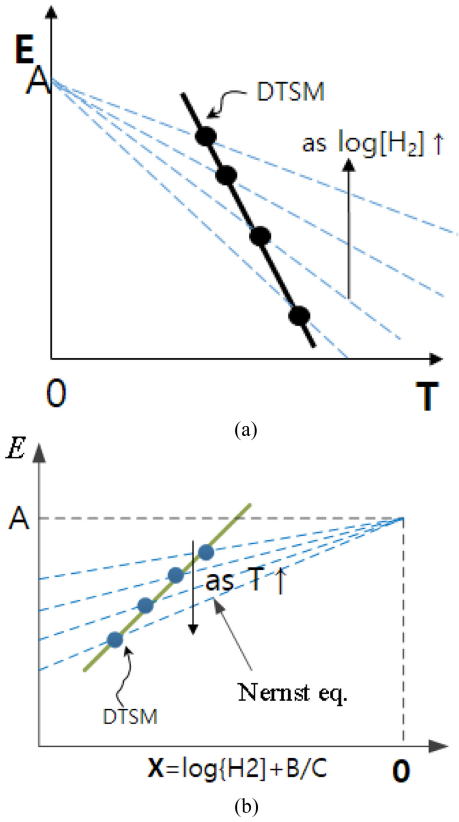

Fig. 7. (a) E vs T and (b) E vs x(=log[H_2]+B/C)

isothermal lines decrease.

In summary, the 3D shape of the sensor output EMF in Eq. 8 may be expressed as a twisted plane in the T-x space, where the projection to the E-T plane gives Fig. 7(a), and the projection to the E-x plane (-x is utilized here for convenience) becomes Fig. 7(b). All the EMFs measured from the hetero-ionic junction sensor were placed on this twisted plane. The projections of the measured data into the E-T and E-x spaces give the linear lines in Figs. 7(a) and (b), respectively.

2.2 Phenomenological Understanding of Response

When the sensor was immersed in the heated vertical furnace, the sensor's temperature (right axis) increased; accordingly, the EMF (left axis) varied. Typical EMF and temperature behaviors are presented in Fig. 9. This is the case where the sensor is dipped in a chamber at 600 ℃ with a gas phase of 2%H_2–98%N_2. EMF starts to rise from around 250 ℃, and there appears to be a jump at approximately 110 to 200–500 mV (Region I), but this depends on the environment to which the sensor is exposed. A high H_2 concentration environment resulted in a larger jump than that in a low H_2 concentration environment. Subsequently, at least three

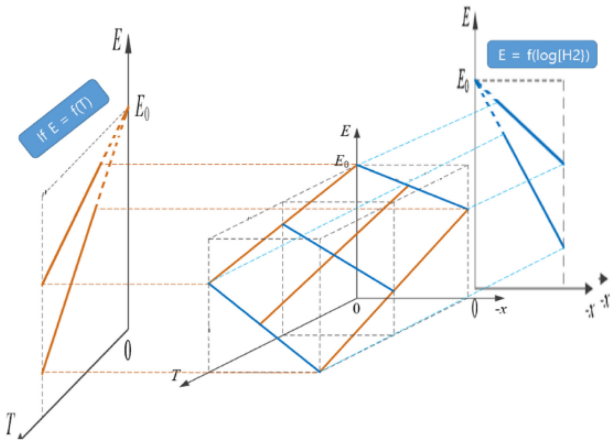

Fig. 8. Sensor EMF as function of T and -x

humps (Regions II, III, and IV) appear before the final steady-state EMF is reached. This differs from the EMF behavior obtained from the YSZ oxygen sensor, which exhibits a smoothly rising curve [15]. In a high H_2 concentration environment, Region III often disappears.

This phenomenon is suspected to be related to the following two-step process. In the early stage of Region Ⅱ, the oxygen and the incoming hydrogen react together to make a surface oxygen adsorbate and proton by the reaction:

$$\frac{1}{2}O_2+H_2=O_O^X(surface)+2H^++2e \quad (11)$$

The proton in Reaction 11 gives an early EMF of Region Ⅱ at a temperature of around 250–400 ℃. As the sensor's temperature increases with time, two possible processes may occur that produce a measurement output in late Stages III and IV. The first possibility is that as oxygen is depleted near the CZI, the incoming hydrogen starts to react with the oxygen adsorbate in Eq. 11 to produce oxygen vacancies ($V_o^{\cdot\cdot}$) by the reaction:

$$O_O^X(surface)+H_2=V_O^{\cdot\cdot}+H_2O+2e \quad (12)$$

The oxygen vacancies in Reaction 12 produce Region III or IV EMF wave depending on the hydrogen concentration in the melt.

The second possibility is the equilibrium reaction at the electrode between hydrogen and the proton on CZI, as indicated in Reaction 13.

$$H_2=2H^++2e \quad (13)$$

The proton in Eq. 13 results from the oxygen vacancies formed by the substitutional reaction of In into the Zr sites in $CaZrO_3$, as expressed in Eq. 14.

$$In_2O_3=2In_{Zr}^{'}+3O_O^X+V_O^{\cdot\cdot} \quad (14)$$

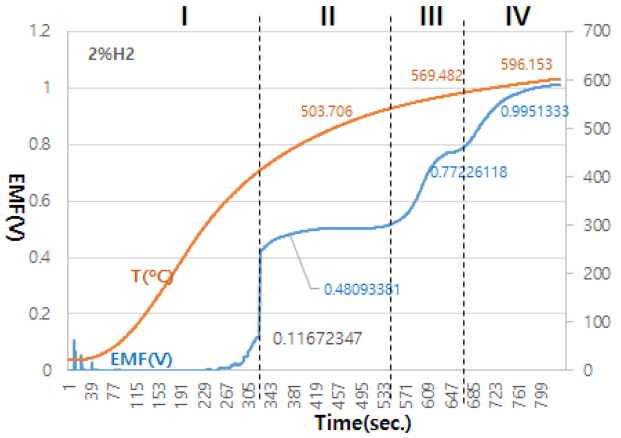

Fig. 9. Typical EMF and temperature behaviors of sensor immersed in system in 2%H_2-N_2 atmosphere at 600 °C.

These oxygen vacancies play a role in converting hydrogen gas into protons via the following reaction.

$$H_2 + V_o^{\cdot\cdot} = (2H)_O^{\cdot} \quad (15)$$

where $(2H)_O^{\cdot}$ is proton bound to oxygen vacancy.

3. RESULTS AND DISCUSSION

We ran ten sets of experiments, as presented in Table 1, by immersing the sensor into the preheated furnace of Fig. 4(b) to obtain the corresponding sets of EMF and temperature for a given hydrogen concentration ranging from 2% to 9%. The measurements were performed by obtaining the EMF, Es, and the corresponding temperature, Ts, when the EMF was stabilized. In contrast, the sensor's temperature increased upon dipping the sensor into the furnace. Here, the sensor was inserted into the furnace at two different temperatures of 600 and 650 °C to give a different heating rate.

Table 1. Ten sets of EMFs and temperatures measured from two different reactor conditions and changing hydrogen concentration from 2% to 9%.

Experiment Number	Injected [H_2]	Ts(K)	Es(mV)
1	2%	849	952
2	2%	888	930
3	4%	837	969
4	4%	857	966
5	5%	804	997
6	5%	866	970
7	7%	791	1019
8	7%	819	1000
9	9%	778	1033
10	9%	815	1017

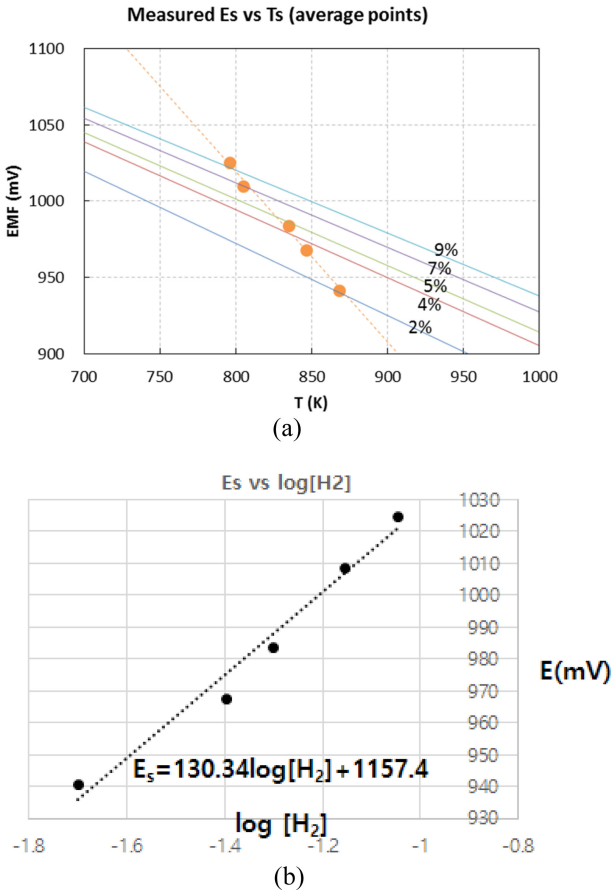

Fig. 10. (a) E_s plotted on T axis and (b) E_s vs log[H_2]

We created more datasets and plotted them in the 3D space of E-T-log[H_2], as illustrated in Fig. 11. The data points appeared to lie on a flat plane rather than a twisted plane. Our experimental conditions were so narrow that it was assumed they sat on a plane.

In this case, we can obtain A, B, and C analytically from Eq. 8, by solving the following differential equation:

$$dE/dT = K \quad (13)$$

with two boundary conditions of

$$E = M\log[H_2] + L \quad (14)$$

and

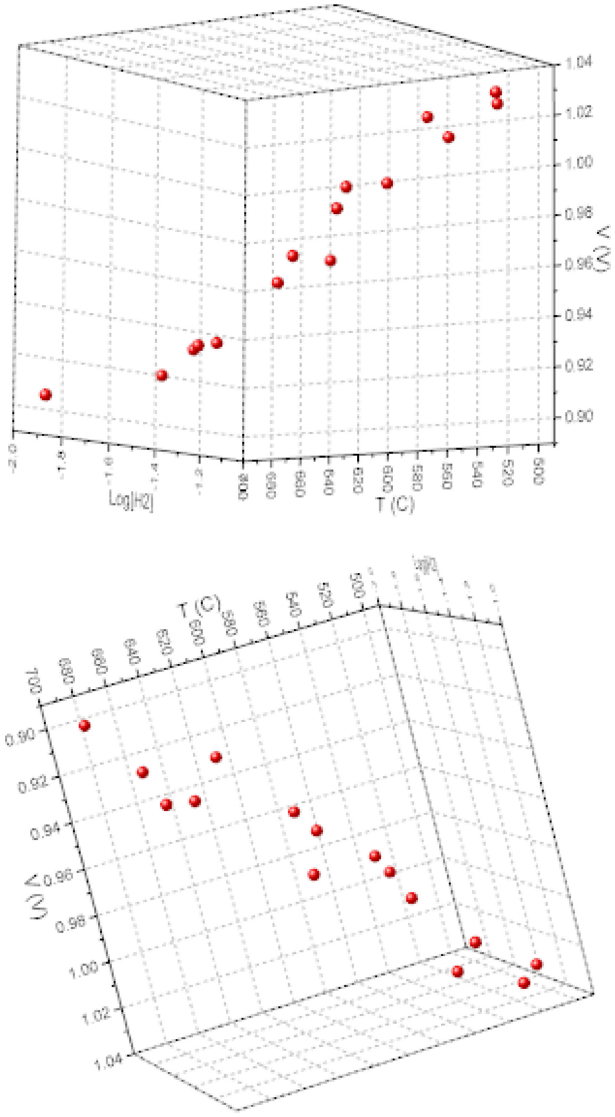

Fig. 11. Plot of (E_i,T_i, log[H_2]$_i$) in 3-D space of T-log[H_2]-E

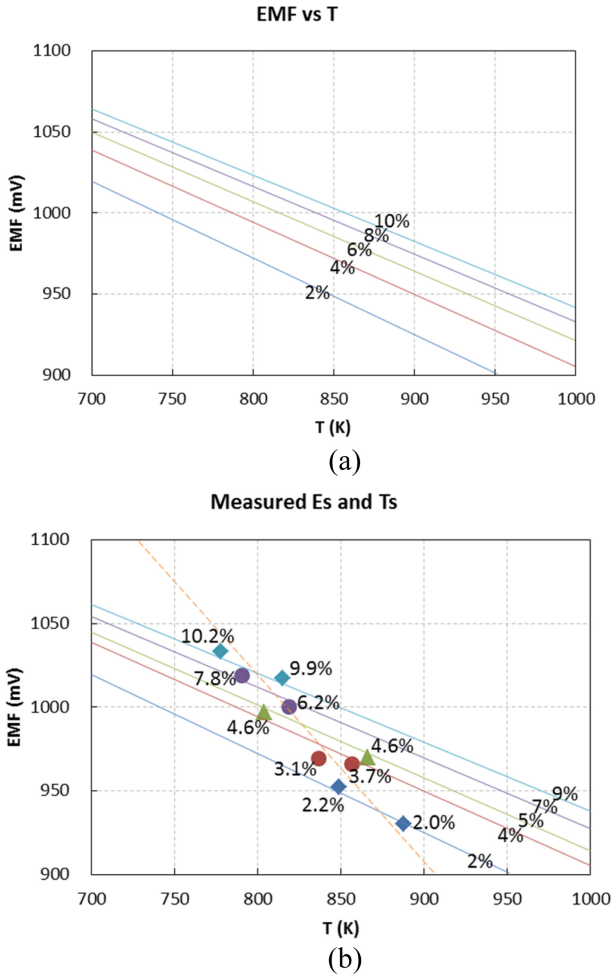

Fig. 12. (a) EMF as function of temperature for different hydrogen concentrations and (b) (Es, Ts) plotted on E-T space.

$$T = \alpha \log[H2] + \beta \quad (15)$$

Here, K can be obtained from the experimental data in Fig. 10(a), and M and L can be obtained from Fig. 10(b). And α and β can also be obtained by plotting data on the E vs log[H_2] diagram. Therefore, the hydrogen concentration can be obtained utilizing Eq. 16, as long as we clear K, M, L. α, and β from the experiment.

$$\mathrm{Log}[H_2] = (E - KT - L + \beta K)/(M - \alpha K) \quad (16)$$

4. CONCLUSIONS

A heterojunction solid electrochemical sensor responds selectively to hydrogen gas over 400 ℃. It demonstrates a stable interfacial structure of YSZ/CZI irrespective of temperature and hydrogen atmosphere and gives an output expressed as E= A + BT + CT log[H_2]. Generally, the EMF behavior exhibits a jump and three humps before reaching a final value corresponding to the relevant hydrogen concentration. This may have resulted from the reaction of hydrogen with the remaining oxygen to form an oxygen adsorbate.

The configuration of the heterojunction sensor is convenient for measuring dissolved hydrogen in the liquid phase because its simple reference electrode arrangement makes a hermetically sealed chamber easy. In addition, because all components are made of stable oxide ceramics, they can withstand harsh environments. The heterojunction sensor is expected to be applied in a wide variety of areas owing to its versatility and simplicity of structure, for example, as a hydrogen sensor for leakage detection, dissolved hydrogen measurement for molten Al alloys, dissolved hydrogen gas analysis for transformer oil, etc.

ACKNOWLEDGMENT

This work was supported by the Daedok Innopolis R&BD Project and the MSIT as GFP/CISS 2011-0031870. I would also like to thank Prof. H. J. Yoo for the helpful discussions on the derivation of the mathematical algorithm.

REFERENCES

[1] T. Hubert, L. Boon-Brett, G. Black, and U. Banach, "Hydrogen Sensors-A Review", *Sens. Actuators B Chem.*, No. 157, No. 2, pp. 329-352, 2011.

[2] M. Anand, "Study of tin oxide for hydrogen gas sensor applications", M. S. thesis, University of South Florida, Florida, 2005.

[3] N. S. Baik, G. Sakai, N. Miura, and N. Yamazoe, "Hydrothermally treated sol solution of tin oxide for thin-film gas sensor", *Sens. Actuators B Chem.*, Vol. 63, No. 1-2, pp. 74-79, 2000.

[4] N. Yamazoe, K. Suematsu, and K. Shimanoe, "Surface chemistry of neat tin oxide sensor for response to hydrogen gas in air", *Sens. Actuators B Chem.*, Vol. 227, pp. 403-410, 2016.

[5] Y. Chao, S. Yao, W. J. Buttner, and J. R. Stetter, "Amperometric sensor for selective and stable hydrogen measurement", *Sens. Actuators B Chem.*, Vol. 106, No. 2, pp. 784-790, 2005.

[6] S. W. Jung, E. K. Lee, and S. Y. Lee, "Communication-Concentration cell type Nafion-based potentiometric hydrogen sensors", *ECS J. Solid State Sci. Technol.*, Vol. 7, No. 12, pp. Q239-Q241, 2018.

[7] I. Lundstrom, S.Shivaraman, C. Svensson, and L. Lundkvist, "A hydrogen-sensitive MOS field-effect transistor", *Appl. Phys. Lett.*, Vol. 26, No. 2, pp. 55-57, 1975.

[8] F. A. Lewis, *The Palladium Hydrogen System*, Academic Press, London, New York, pp. 21-36, 1967.

[9] G. Lu, N. Miura, and N. Yamazoe, "High-temperature hydrogen sensor based on stabilized zirconia and a metal oxide electrode", *Sens. Actuators B Chem.*, Vol. 35, No. 1-3, pp. 130-135, 1996.

[10] T. Yajima, K. Koide, H. Takai, N. Fukatsu, and H. "Iwahara, Application of hydrogen sensor using proton conductive ceramics as a solid electrolyte to aluminum casting industries", *Solid State Ion.*, Vol. 79, pp. 333-337, 1995.

[11] C. Schwandt, "Solid state electrochemical hydrogen sensor for aluminium and aluminium alloy melts", *Sens. Actuators B Chem.*, Vol. 187, pp. 227-233, 2013.

[12] B. H. Jung, "Hydrogen Measurement in Al Melt at 720oC", Ph. D thesis, KAIST, Daejeon, 2013.

[13] C. Schwandt, "Comment on the article 'New solid-state electrochemical method of measuring dissolved hydrogen in Al melt' by S.G. Kim, B.H. Jung, C.O.Park, R.A. Rapp", *Sens. Actuators B Chem.*, Vol. 255, No. 2, pp. 2066-2068, 2018.

[14] S. G. Kim, B. H. Jung, C. O. Park, and R. A. Rapp, "New solid-state electrochemical method of measuring dissolved hydrogen in Al melt", *Sens. Actuators B Chem.*, Vol. 239, pp. 374-382, 2017.

[15] Y. C. Yang and C. O. Park, "Oxygen sensor for the low temperature-measurement using yttria stabilized zirconia(YSZ) electrolyte and Ag electrode", *J. Sens. Sci. Technol.*, Vol. 15, No. 2, pp. 97-101, 2006.

[16] K. Young and D. W. Cleaves, "Determination of hydrogen in titanium metal by hot extraction", *Anal. Chem.*, Vol. 28, No. 3, pp.372-374, 1956.

[17] A. M. Samuel and F. H. Samuel, "The reduced pressure test as a measuring", *Metall. Trans. A*, Vol. 24, pp. 1857-1868, 1993.

[18] P. D. Waite, "Improved metallurgical understanding of the Alcan compact degasser after two years of industrial implementation in aluminum casting plants", *Light Metals Warrendale*, pp. 791-796, 1998.

[19] F. Paray, *In Situ Hydrogen Measurements in Liquid Al-Si foundry Alloys.*, McGill University, Quebec, 1996.

[20] JANAF Thermodynamic Table.